2016

Localised magmatic constraints on continental back-arc volcanism in southern Mendoza, Argentina: the Santa Maria Volcano

Venera Espanon
University of Wollongong, vre981@uowmail.edu.au

Allan Chivas
University of Wollongong, toschi@uow.edu.au

Simon P. Turner
Macquarie University

Leslie Kinsley
Australian National University, leslie.kinsley@anu.edu.au

Anthony Dosseto
University of Wollongong, tonyd@uow.edu.au

Publication Details

Espanon, V. R., Chivas, A. R., Turner, S. P., Kinsley, L. P. J. & Dosseto, A. (2016). Localised magmatic constraints on continental back-arc volcanism in southern Mendoza, Argentina: the Santa Maria Volcano. Bulletin of Volcanology, 78 (11), 83-1-83-13.

Localised magmatic constraints on continental back-arc volcanism in southern Mendoza, Argentina: the Santa Maria Volcano

Abstract
The Payún Matrú Volcanic Field constitutes part of the continental back-arc in Argentina. This volcanic field has been the focus of several regional investigations; however, geochemical analysis of recent volcanoes (<8>ka) at the scale of an individual volcano has not been conducted. We present a morphological description for the Santa Maria Volcano in addition to results from major and trace element analysis and 238U-230Th-226Ra disequilibria. The trace element evidence suggests that the Santa Maria magmatic source has a composition similar to that of the local intraplate end member (resembling an ocean island basalt-like source), with a slight contribution from subduction-related material. The U-series analyses suggest a high 226Ra excess over 230Th for this volcano, which is not derived from a shallow process such as hydrothermal alteration or upper crustal contamination. Furthermore, intermediate-depth processes such as fractional crystallisation have been inferred for the Santa Maria Volcano, but they are not capable of producing the 226Ra excess measured. The 226Ra excess is explained by deep processes like partial melting of mantle lithologies with some influence from subducted Chilean trench sediments. Due to the short half-life of 226Ra (1600 years), we infer that fast magma ascent rates are required to preserve the high 226Ra excess.

Disciplines
Medicine and Health Sciences | Social and Behavioral Sciences

Publication Details
Espanon, V. R., Chivas, A. R., Turner, S. P., Kinsley, L. P. J. & Dosseto, A. (2016). Localised magmatic constraints on continental back-arc volcanism in southern Mendoza, Argentina: the Santa Maria Volcano. Bulletin of Volcanology, 78 (11), 83-1-83-13.

Localised magmatic constraints on continental back-arc volcanism in southern Mendoza, Argentina: The Santa Maria volcano

Venera R. Espanon [a,b,*], Allan R. Chivas[a], Simon P. Turner[c], Leslie P.J. Kinsley[d] and Anthony Dosseto[a,b]

[a] *GeoQuest Research Centre, School of Earth & Environmental Sciences, University of Wollongong, NSW 2522, Australia.*

[b] *Wollongong Isotope Geochronology Laboratory, School of Earth & Environmental Sciences, University of Wollongong, NSW 2522, Australia.*

[c] *Department of Earth and Planetary Sciences, Macquarie University, Sydney, NSW 2109, Australia.*

[d] *Research School of Earth Sciences, The Australian National University, Canberra, ACT 0200, Australia.*

**Current address: Institute of Earth and Environmental Sciences – Geology, University of Freiburg, Freiburg 79104, Germany.*

Allan R. Chivas: toschi@uow.edu.au

Simon P. Turner: simon.turner@mq.edu.au

Leslie J. Kinsley: leslie.kinsley@anu.edu.au

Anthony Dosseto: tonyd@uow.edu.au

Acknowledgments

We acknowledge the Renewable Natural Resources division of the Province of Mendoza for providing access permits. We greatly thank the park rangers at Llancanelo and Payunia Provincial Natural Reserves (Mendoza) and Leandro Rojo, Luis Lopez, Daniel Espanon and Ryan Manton for their assistance during field trips. We thank Norman Pearson from Macquarie University for his contribution with the laboratory analysis. We are grateful to Olgeir Sigmarsson for his constructive comments and suggestions. The fieldwork component of this study was funded, in part, by a short-term mobility scholarship to A.R. Chivas and V.R. Espanon for field training in young geological processes from the then Department of Industry, Innovation, Science, Research and Tertiary Education of the Australian Government. Anthony Dosseto acknowledges Australian Research Council Future Fellowship FT0990447.

Keywords

Back-arc basalts, U-series, ^{226}Ra excess, Payenia Basaltic Province, Andean Southern Volcanic Zone.

Abstract

The Payún Matrú Volcanic Field constitutes part of the continental back-arc in Argentina. This volcanic field has been the focus of several regional investigations; however, geochemical analysis of recent volcanoes (<8 ka) at the scale of an individual volcano has not been conducted. We present a morphological description for the Santa Maria volcano in addition to results from major- and trace- element analysis and ^{238}U-^{230}Th-^{226}Ra disequilibria. The trace-element evidence suggests that the Santa Maria magmatic source has a composition similar to that of the local intraplate end member (resembling an OIB-like source), with a slight contribution from subduction related material. The U-series analyses suggest a high ^{226}Ra excess over ^{230}Th for this volcano, which is not derived from shallow process such as hydrothermal alteration or upper crustal contamination. Furthermore, intermediate depth processes such as fractional crystallization have been inferred for the Santa Maria volcano, but they are not capable of producing the ^{226}Ra excess measured. The ^{226}Ra excess is explained by deep processes like partial melting of mantle lithologies with some influence from subducted Chilean trench sediments. Due to the short half-life of ^{226}Ra (1600 years), we infer that fast magma ascent rates are required to preserve the high ^{226}Ra excess.

1. Introduction

Continental back-arc volcanism is associated with areas where the subducting slab is located at greater depth than at the volcanic arc front, and which are therefore, less likely to be influenced by fluids released through dehydration of the subducting slab (Schmidt and Poli 1998). The volcanism in the Payún Matrú Volcanic Field (PMVF) in southern Mendoza, Argentina takes place in a back-arc setting.

The chemical composition of continental back-arc basalts may be influenced by several processes such as contamination by lower continental crust (Søager et al. 2013; Espanon et al. 2014a), slab partial melts (Sigmarsson et al. 2002; Jacques et al. 2013) and the continental lithospheric mantle (Varekamp et al. 2010). This heterogeneity has been previously identified in Patagonian continental back-arc basalts, such as in the Loncopue graben (LP, Figure 1a; Varekamp et al. 2010) and in the Payenia Basaltic Province (Søager et al. 2013, Jacques et al. 2013, Espanon et al. 2014a). In order to distinguish among these processes and sources, an isolated cinder cone, the Santa Maria volcano, and its associated basaltic flow have been chosen for the current investigation. In addition, U-series analysis have been for the first time applied to the PMVF and to this volcano. This method, applied to volcanic rocks, has proved to efficiently assess physical process of Earth's surface and mantle, over different time scales, through isotopic fractionation within the U-series decay chain. The purpose of this investigation is to determine the processes that have affected the geochemical composition of this Holocene volcano in order to obtain a better understanding of recent magmatic processes in this volcanic field.

2. Geological Setting

78 The Payún Matrú Volcanic Field (PMVF) is part of the Payenia Basaltic Province
79 (PBP, Figure 1a). The PBP is the largest and the northernmost Quaternary
80 continental back-arc province of the Andean Southern Volcanic Zone (SVZ). This
81 basaltic province is located in central-west Argentina and is composed of several
82 Pleistocene volcanic fields. Holocene volcanism in the PBP is not abundant, but it
83 has been recognised in a restricted area in the western part of the PMVF (Germa et
84 al. 2010; Gudnason et al. 2012; Espanon et al. 2014b). This volcanic field is located
85 approximately 450 km from the Peru-Chile trench and displays minimal to no
86 subduction-related geochemical signature (Germa et al. 2010; Søager et al. 2013;
87 Espanon et al. 2014a) and has intraplate signatures associated with an enriched
88 upwelling mantle similar to OIB (Germa et al. 2010; Jacques et al. 2013; Søager et
89 al. 2015b).

90 The Santa Maria cinder cone and its associated basaltic a'a flow is located in the
91 central northern part of the PMVF (Figure 1) and to the north-west of the Payún
92 Matrú caldera. This cinder cone and flow corresponds to the younger part of the
93 PMVF (Germa et al. 2010). A reliable age for the Santa Maria volcano has not been
94 determined and the only available ages come from a basaltic flow and bomb, using
95 surface exposure dating based on cosmogenic ^{3}He and ^{21}Ne isotopes (Espanon et
96 al. 2014b). The calculated ages suggest that this volcano is <8ka, which is critical
97 for the ^{226}Ra - ^{230}Th system as after ~5 half-lives (^{226}Ra half-life is 1600 years) it will
98 return to secular equilibrium, hence no ^{226}Ra excess can be detected. The available
99 geochemical data from the Santa Maria volcano are restricted to a single sample
100 taken from the Santa Maria flow to the west of its volcanic cone, and is classified as
101 a trachybasalt (Søager et al. 2013).

102 **3. Methods**

A total of twelve samples from Santa Maria corresponding to basaltic rocks from the flow, cone, scoria and a basaltic bomb, were analysed for major- and trace-elements. Six rock samples were analysed for U-Th–Ra isotopes and two samples were analysed for Sr-isotopes (Table 1).

3.1. XRF and laser ablation procedure

Samples were cleaned and crushed using a Cr-Ni N.V. TEMA rock crusher at the School of Earth and Environmental Sciences, University of Wollongong. The rock powder was mixed with a flux (a mixture of 35.3% lithium tetraborate and 64.7% lithium metaborate) and fused in order to produce a glass disc for each sample. The glass discs were analysed for major elements using a Spectro Xepos energy dispersive polarization X-ray spectrometer at the institution above mentioned. The accuracy of the measurement was monitored using a natural standard (dolerite) W-2 (n=2) (Gladney and Roelandts 1988), with a relative deviation from the recommended values of <3% for all major elements. Loss on ignition was measured using approximately 1 g of powder sample in a furnace at 1050°C, for two hours.

Trace elemental analysis for two samples, VRE51 and VRE52 were performed using X-ray fluorescence spectrometry. Samples were pressed into a pellet using a PVF binder and were analysed using the spectrometer mentioned in the previous paragraph. The remaining samples were analysed for trace elements by laser ablation inductively-coupled plasma mass spectrometry (LA ICP-MS) at the Research School of Earth Sciences, Australian National University. The laser employed was an Excimer laser (ArF 193 nm) 50mJ, 5Hz at a scan rate of 10 microns per second and a spot diameter of 105 μm. The aerosols released were immediately analysed on an Agilent 7200 quadrupole ICP-MS. The samples were

analysed under the same conditions with standard NIST612 (n=6) (GeoReM reference material; Jochum et al., 2011) and data were calibrated according to this standard. The accuracy and reproducibility of the analysis was monitored using two standards (BCR-2, n=7; USGS; Wilson, 1997 and NIST610, n=7; GeoReM reference material; Jochum et al., 2011) analysed as unknowns. The relative standard deviation for most elements is less than 5% (2σ) for the two standards.

3.2. Sr isotope analysis

Sr isotopic analysis was conducted on 2 samples (Table 1). Approximately 0.1 g of powder sample was dissolved in 1.5 mL 30% HCl, 2mL 70% $HClO_4$, 0.5 mL 65% HNO_3 and 2 mL 48% HF, at 130ºC for 12 hours. The samples were dried, re-dissolved in 2M HNO_3 then loaded on a cation exchange column packed first, with 0.1 mL Eichron pre-filter® resin overlain by 0.2 mL Eichrom Sr-spec® resin (Moffat, 2013). Sr was eluted in 0.02M HNO_3 (Moffat, 2013). The Sr isotopic analysis was conducted using a ThermoScientific Neptune multi-collector ICP-MS at the Research School of Earth Sciences, Australian National University. The precision of the Sr isotopic measurements was monitored by the SRM987 standard. The $^{87}Sr/^{86}Sr$ obtained for SRM987 is 0.71034 ± 0.000007 (2σ) which is within the recommended value ($^{87}Sr/^{86}Sr$ = 0.71034 ± 0.00026, National Institute of Standards and Technology, standard reference material 987). Total procedural blank for Sr is 52.4 pg which represents <0.003% of the total Sr analysed and was measured on an Agilent 7500cs quadrupole ICP-MS, at the School of Earth and Environmental Sciences, University of Wollongong.

3.3. U-series

3.3.1 – Separation procedure

Sample preparation was done at the Wollongong Isotope Geochronology Laboratory, University of Wollongong. Approximately 0.3 g and 0.02 g of ^{228}Ra and ^{229}Th-^{236}U tracer solutions, respectively, were added to 0.6-1.4 g of ground sample prior to digestion. Samples were digested using the same volume and concentrations as in section 3.2. The samples were then re-dissolved in a H_3BO_3-saturated solution of 6M HCl and boric acid and left to react for several hours at 120°C in order to dissolve any insoluble fluorides (Koornneef et al. 2010). After evaporation of the H_3BO_3-saturated solution, the samples were re-dissolved in 7.5M HNO_3. Uranium, Th and Ra were then separated using a series of solid-liquid chromatography columns packed with ion exchange resins. The U-Th and Ra separation procedure was modified from Luo et al. (1997) and Claude-Ivanaj et al. (1998), respectively.

3.3.2 – Analytical procedure

The Ra fraction was loaded on a Re filament in Ta oxide and analysed on a Thermo Finnigan Triton® Thermal Ionization Mass Spectrometry (TIMS) at GEMOC, Department of Earth and Planetary Sciences, Macquarie University. Uranium and Th concentrations were measured on a Thermo Neptune Plus® multi-collector ICP-MS at the Research School of Earth Sciences, Australian National University. The procedural blank was <2 fg for Ra, while for Th it was 78 ± 12 pg (n=2) and for U, 43 ± 3 pg (n=2). The ^{226}Ra standard used was within 1% of the recommended value (433 fg/g). Three individual aliquots of BCR-2 rock standard were digested and used throughout the separation procedure and analysis, to assess the accuracy and reproducibility, with a relative standard deviation of 1% for Th, U and Ra and within error of previous published values (Wilson, 1997; Koornneef et al. 2010; Reubi et al. 2014). The (^{230}Th/^{232}Th) and (^{234}U/^{238}U) (parentheses denote activity ratio) were within 1.5% of previously published values, while (^{230}Th/^{238}U) and (^{238}U/^{232}Th) were

within 5.5% of previous published values (Sims et al. 2008; Reubi et al. 2014). In the case of ($^{226}Ra/^{230}Th$), the measured value was within 4% of the recommended value for BCR-2 (Koornneef et al. 2010; Reubi et al. 2014).

4. Results

4.1. Geomorphological description of the Santa Maria cone and flow

Santa Maria is a monogenetic volcano with a well-preserved scoria cone breached to the north-west. The main cone is composed of two craters and one small scoria cone on the south-eastern side of the main cone. This volcano is located at 1940 MASL and rises 140 m above the surrounding topography. The basaltic a'a flow extends for 16.5 km from the cone in a north-easterly direction with a topographic slope of 1.97% covering an area of 42.4 km^2 with a volume of 0.94 km^3 (calculated using the method described in Espanon et al. 2014c). The Santa Maria cone has high slope angles (>30°; Figure 2a) related to young volcanic activity, as generally, the angle decreases with time due to erosion. Furthermore, the scoria ejected has been preserved in place on the southern and north-eastern side of the cone, the basaltic bombs ejected have also been preserved and deposited on the southern side of the cone. The bomb size ranges up to almost a metre, most have a near-spherical shape, while there are some examples of spindle, ribbon and bread-crust bombs (Figure 2b, c). The main volcanic cone has several spatter ramparts (Figure 2d) which suggest an eruption event similar to a volcanic fountain, while on the north-western side of the cone there is a fissure vent (Figure 2d) which is currently covered by red scoria (sample SM9). These effusion points have been previously interpreted as the migration of the eruptive vent when the system was active (Risso et al. 2006).

On the top of the cone, a clay-rich area with lighter colour is likely to be the remnants of a fumarole or a solfatara (Figure 2e).

The morphology of the Santa Maria volcano suggests that the eruption had a Hawaiian style, which then developed into a strombolian style in order to produce the scoria and basaltic bomb field. The different colours within the Santa Maria flow (Figure 1c and Figure 2f) are identified as several potential generations of basaltic flows. At least two generations were identified in the field and are recognised on the satellite image (Figure 1c). The first represented by the lighter brown colour, is slightly vegetated and colonised by lichen (Flow 1, Figure 2f). The second (Flow 2) is represented by the dark brown/black colour of the inner channel (Figure 1c), lacks vegetation/lichen and it is stratigraphically above Flow 1. Samples SM3, SM4, SM7, SM6 and SM10 possibly belong to Flow 2 (other samples have not been assigned to either of the flows, as it is ambiguous to which flow generation they belong). A'a is the dominant lava type for the Santa Maria flow (Figure 2g); however, there are some structures such as lava ridges and tube-like structures (Figure 2h), suggesting that at some stage the lava was less viscous.

4.2. Petrography of the Santa Maria flow

The basalts from Santa Maria are vesicular and the dominant texture is porphyritic. However, some samples have a seriate or less commonly a glomeroporphyritic texture. The most abundant phenocrysts are plagioclase and olivine, with low abundance of clinopyroxene microcrysts. Most of the olivine phenocrysts have euhedral to subhedral crystal shape; while samples SM10 and SMT3 present skeletal olivine and sample VRE51 has sparse anhedral olivine. The plagioclase

phenocrysts are commonly euhedral and show multiple twinning while some show oscillatory zoning. Alteration is not evident and phenocrysts boundaries are sharp.

4.3. Major- and trace-element results and Sr-isotopic results

Major-element concentrations show a narrow range of values. Most of the samples are alkaline trachy-basalt, while samples SM9 and SM12 which are scoria samples classified as basalts, according to the total alkalis versus silica classification (Le Bas et al. 1986).

Rare Earth Element (REE) contents normalised to chondrites (Boynton 1984) show a smooth pattern with fractionation of the heavy rare earth elements (HREE; Figure 3a). The Santa Maria samples have the highest La/Sm ratios of all the samples from PMVF (Espanon et al. 2014a) ranging from 4.01 to 3.46 and the lowest Dy/Yb ranging from 2.03 to 2.24. On Figure 3a, samples show patterns below the average ocean island basalt (OIB) composition end-member (Sun and McDonough 1989) and are within the local OIB-like field (Rio Colorado field from, Søager et al., 2013).

The trace element data for the Santa Maria samples and an average arc composition (average compiled from the Andean volcanic arc with <53 SiO_2 wt % between 35°S and 38°S, see Figure 3) were normalised to primitive mantle composition (McDonough and Sun 1995) in order to compare the composition of Santa Maria rocks to those of the Andean volcanic arc on Figure 3b. The Santa Maria rocks show enrichment in highly incompatible elements (Cs, Rb, Ba, Th, U) while Nb shows a slight negative anomaly. The average Nb/Ta value for these samples is 16.8 which is relatively high when compared to other samples in the PMVF but it is lower than the Rio Colorado as it has a positive Nb-Ta (Figure 3b). The $^{87}Sr/^{86}Sr$ isotopic composition shows little variation between the two samples analysed (SM4,

0.703861 and SM10, 0.703867; Table 1) and the values are comparable to previously reported Sr-isotopic values for PMVF (Hernando et al., 2012; Jacques et al., 2013; Pasquarè et al., 2008; Søager and Holm, 2013; Espanon et al., 2014a).

4.4. U-series isotopes

The results from the U-series analysis show that Santa Maria lavas have restricted Ra concentrations, from 433 to 493 fg/g (Table 2). The ($^{230}Th/^{232}Th$) and ($^{238}U/^{232}Th$) from Santa Maria have a restricted range from 0.92 to 0.95 and from 0.91 to 0.94, respectively (Table 2). The results for these two activity ratios are illustrated on an equiline diagram (Figure 4a; Condomines and Sigmarsson 1993). Generally, rocks from intraplate or mid-ocean ridge settings tend to be on the left side of the equiline while convergent margin samples tend to have a shift to the right of the equiline as a ^{238}U excess is associated with fluid addition from dehydration of the subducting slab (Turner et al. 2003). The restricted range in ($^{230}Th/^{232}Th$) and ($^{238}U/^{232}Th$) of the Santa Maria volcano plots close to secular equilibrium (cf. Condomines and Sigmarsson 1993).

The ($^{234}U/^{238}U$) ratios also show little deviation from secular equilibrium except for sample SM7 that has a ($^{234}U/^{238}U$) ratio of 1.034 ± 0.006 (Table 2, Figure 4b). The ($^{226}Ra/^{230}Th$) activity ratios range from 1.27 to 1.73 (Table 2), which is similar to the range observed in intraplate settings (OIB ≤ 1.7), based on values from Hawaii and the Canary Islands from Sims et al. (1999) and Lundstrom et al. (2003), respectively. The ($^{226}Ra/^{230}Th$) ratios from the Santa Maria samples are positively correlated with Rb/Th (Figure 4c) Nb/U, Ba/Th, Nb/Th and Zr/U but negatively correlated with Th concentration (Figure 4d). Note that the measured ($^{226}Ra/^{230}Th$) activity ratios are considered minimum values because the eruption ages are unknown. Therefore, the

following discussion focuses on the origin of ^{226}Ra excess rather than the range of measured values.

5. Discussion

5.1. Geochemistry of the Santa Maria Volcano

The Santa Maria volcano has been investigated in order to better understand the processes that have contributed in forming this young (<8 ka) basaltic flow. The geochemistry of its rocks indicates that they are enriched in the most incompatible elements and their compositions are similar to those of intraplate magmas, in this case similar to the local OIB-like source here represented by the Rio Colorado Volcanic Field from Søager et al., 2013 (Figure 3a, 3b). The samples have high contents of High Field Strength Elements (HFSE) comparable to those described in Espanon et al. (2014a) for Los Volcanes group also part of the PMVF (Figure 1b). Contamination by lower continental crust (LCC) has been proposed previously as one of the processes modifying the geochemical signatures observed in the Payenia Basaltic Province, especially in the Nevado Volcanic Field (Søager et al. 2013) and in the PMVF (Figure 1b; Søager et al. 2013; Espanon et al. 2014a). Gabbroic cumulates located at lower continental crust level have high Ba/Th and Nb/U and low U/Pb (Søager and Holm, 2013). The samples from this volcano present the lowest Ba/Th and Nb/U at the highest U/Pb ratios (Figure 5a) from the PMVF, therefore suggesting that lower crustal contamination is not likely to be a process affecting the geochemical characteristic of the lavas erupted from this volcano. Furthermore, upper continental crust contamination is not suggested for this volcano as the Sr-isotopes here determined agree with previous determined values for the PMVF (Pasquarè et al., 2008; Hernando et al., 2012; Jacques et al., 2013; Søager and

294 Holm, 2013; Espanon et al., 2014a). Nevertheless, the relatively young continental
295 crust in this area has been identified as having a small isotopic contrast with the
296 mafic lavas (Gerlach et al., 1988), suggesting that the $^{87}Sr/^{86}Sr$ ratio may not be an
297 entirely suitable parameter. However, $\delta^{18}O$ values from two olivine phenocrysts from
298 young basalts located approximately 10 km from Santa Maria volcano indicate a
299 mantle origin (samples CL 360 and CL 372 with, $\delta^{18}O$ of 5.02 ± 0.02 and 5.06 ± 0.10
300 respectively from Jacques et al. 2013) also implying that continental crustal
301 contamination did not affect these samples.

302 Considering the tectonic setting of the Santa Maria volcano, any subduction-related
303 signature in the back-arc, is not expected to be derived directly from fluids released
304 from dehydration of the subducting slab. In this region of the back-arc the subducting
305 slab has been inferred to be located at approximately 220 km depth (Tassara et al.
306 2006). Hence, it is improbable that at this depth fluids are still departing from the
307 slab. This is also suggested by the low value of fluid-sensitive ratios such as Sr/Th,
308 Ba/Ta, Ce/Pb and Ba/Th observed in the Santa Maria samples. The Ce/Pb, Nb/U
309 and Ba/Th ratios have low values (Figure 5a, 5b), they are actually lower than in the
310 rest of PMVF (data from Espanon et al. 2014a) and in the Rio Colorado volcanic field
311 (data from Søager et al. 2013) associated with a high Pb, U and Th possibly derived
312 from the subducting slab, but not directly from fluids (see following discussion in
313 Section 5.2.3). A possible explanation for this could be that the back-arc is
314 influenced by sediments from the slab in a heterogeneous manner which are
315 capable of transporting not only U and Pb but also Th.

316 The geochemistry of the Santa Maria rocks also suggests that the main flow is
317 composite, as it is composed of several individual volcanic events. This is shown by
318 the good correlation between samples from the proposed flow 2, which includes

samples SM3, SM4, SM7 and SM10 (Figure 4e, 4f). The other two samples VRE51 and VRE52 do not seem to belong to the same volcanic event, because; i) they belong to the area surrounding the Santa Maria cone instead of, from the main basaltic flow and ii) the correlation (r^2) decline in figure 4d, 4e, 4f markedly when these two samples are included. The samples hypothesised to be part of flow 2 (including sample SM6), cluster at low Zr and Y (Figure 5c), while the rest of the samples from this volcano have higher concentrations for these elements. This preliminary geochemical finding supports the hypothesis that the Santa Maria flow does not represent just one basaltic flow but several events at different times during the same eruption, as suggested from the physical nature of this flow (Figure 1c and Section 4.1).

5.2. Assessing the radium excess source

5.2.1. Shallow processes (crustal level)

Hydrothermal activity can result in radioactive disequilibrium between U-series nuclides in igneous rocks. Deviation of ($^{234}U/^{238}U$) from secular equilibrium can be indicative of low-temperature alteration (Figure 4b). Furthermore, hydrothermal activity generally involves the addition of fluid-mobile U to the magma, resulting in ($^{238}U/^{232}Th$) and ($^{230}Th/^{238}U$) being negatively correlated (Villemant et al. 1996). This negative correlation is likely to be accompanied by petrographic observations of alteration in the matrix. Villemant et al. (1996) proposed that ^{238}U-^{230}Th disequilibrium in lavas from the Lesser Antilles could be accounted for by magma mixing or interaction with hydrothermal fluids. In our case, the Santa Maria rocks are characterised by only small ^{238}U-^{230}Th disequilibrium and restricted ranges of ($^{230}Th/^{232}Th$), ($^{238}U/^{232}Th$) (Figure 4a), ($^{230}Th/^{238}U$) and Th/U ratios. Thus, it seems

343 unlikely that hydrothermal activity played a significant role in the U-series isotope
344 composition of these lavas. This is supported by petrographic observations, which do
345 not indicate hydrothermal alteration (e.g., there are no secondary phases present on
346 the rims of the phenocrysts). Low SO_3 concentrations further support the lack of
347 significant hydrothermal activity. Despite mentioning in Section 4.1 that the light
348 coloured altered rock (Figure 2d) could be from an extinct fumarole or a solfatara, all
349 the samples analysed here were fresh basaltic samples from the flow and lacked
350 alteration.

351 Upper crustal assimilation typically results in decreases in U-series isotopic
352 disequilibrium (Berlo et al., 2004) but tends to increase the $^{87}Sr/^{86}Sr$ ratios, which is
353 unlikely as previously mentioned in Section 5.1. Accordingly, hydrothermal alteration
354 and upper crustal assimilation are processes likely not to be responsible for the high
355 Ra-excess in the Santa Maria rocks.

356 5.2.2. Intermediate processes (magma chamber level)

357 Uranium, Th and Ra are strongly incompatible elements in gabbroic minerals.
358 Therefore, accumulation of mafic minerals such as olivine is not capable of affecting
359 the ($^{226}Ra/^{230}Th$), ($^{230}Th/^{232}Th$), ($^{238}U/^{232}Th$) and ($^{230}Th/^{238}U$) ratios. For instance,
360 Vigier et al. (1999) showed that as much as 30% of plagioclase accumulation results
361 in only a slight decrease in ($^{226}Ra/^{230}Th$).

362 The negative correlation between ($^{226}Ra/^{230}Th$) ratios and Th concentrations (except
363 sample SM4) defines a differentiation trend (Figure 4d), also suggested by the
364 weakly positive trends inferred for the Santa Maria samples between K_2O+Na_2O vs
365 SiO_2 and Cr/Th vs MgO (Figure 5d, 5e). The differentiation inferred for the Santa
366 Maria samples is minor as can be seen by the minor SiO_2 increse and MgO

decrease, but it represents a general trend, from which the individual hypothesesed flows are not distinguished. The general trend on Figure 4d of decreasing ($^{226}Ra/^{230}Th$) with increasing Th content is best explained by differentiation over timescales shorter than a few thousand years, such that the ^{226}Ra excess is preserved (Vigier et al., 1999). Despite identifying a weak differentiation trend, it is evident that the magma had a Ra excess before entering the sub-volcanic magmatic chamber.

5.2.3. Deep processes

Radium is a fluid mobile element therefore, at convergent margins, ^{226}Ra and ^{238}U excess are generally associated with dehydration of the subducting slab. However, and as previously mentioned, the subducting slab in the back-arc has been inferred to be deep (220 km, Tassara et al. 2006) and ^{226}Ra excesses are typically not observed in volcanic rocks where the depth of the slab is greater than 110 km (Turner et al. 2003). Furthermore, ^{238}U excess, is not observed in our rocks (Figure 4a, Table 2). Nevertheless, the excess ^{226}Ra can be related to sediments transported by the subducting slab. As can be observed in Figure 5b and 5f the samples from Santa Maria volcano lie on an extrapolation with Chilean trench sediments (Jacques et al., 2013) and the Rio Colorado field. Including the upper continental crust (Rudnick and Gao, 2003) only modifies the r^2 in the 3rd decimal place, hence not affecting the trend line. Nevertheless, when the arc field is included in the extrapolation the r^2 decreases significantly.

Considering the lack of ^{238}U excess, the location of the Santa Maria volcano in relation to the subducting slab and the poor correlation of the Santa Maria samples with the arc end member, we hypothesise that the slab transported sediments are

391 the most probable end member responsible for an arc-signature in the Santa Maria
392 volcano. Slab sediments are capable of transporting not only fluid-mobile elements
393 but also, immobile elements such as Nb, Ta, and Th. If Ba is considered an
394 analogue of Ra, (similar chemical properties; Chabaux et al., 1994) the addition of
395 Chilean trench sediments with relatively high Ba content (1174 ppm, sediment
396 average, Jacques et al. 2013) can provide a feasible explanation for the high Ra and
397 Th content in the back-arc.

398 In typical Ocean island settings, the ($^{226}Ra/^{230}Th$) disequilibrium is derived from
399 partial melting (Gill and Williams, 1990); which is hypothesised to be a process
400 contributing to the high ^{226}Ra excess among the Santa Maria basalts. In addition, the
401 lithospheric mantle thins in the back-arc therefore a decrease in pressure can
402 facilitate the partial melting of peridotite or pyroxenite mantle lithologies.

403 Furthermore, in ocean island settings the ($^{226}Ra/^{230}Th$) disequilibrium is relatively
404 low, as ^{226}Ra decay during ascent or in the magma chamber. The ($^{226}Ra/^{230}Th$) ratios
405 for Santa Maria volcano are just slightly greater than those observed in Hawaiian
406 lavas (Sims et al. 1999), which is remarkable considering that these magmas had to
407 traverse a much thicker crust. In addition, it is hypothesised that the magma resided
408 in the magmatic chamber for a short time and that the magma transport rate was fast
409 in order to preserve the high ^{226}Ra excess. Fast ascent rates are comparable to
410 previous estimates of 10 -100 m/a in continental settings such as in the Southern
411 Volcanic Zone in South America (Sigmarsson et al. 2002). Fast melt transport is
412 better explained by channel flow rather than by equilibrium-porous flow (Turner et al.
413 2001; Sigmarsson et al. 2002), which is easily achieved within the brittle and thin
414 lithospheric mantle.

6. Conclusions

This study constitutes the first attempt to use U-series analysis for the Payenia Basaltic Province, and the first detailed study of a single Holocene volcano in the province. From this investigation we inferred that:

1. The magmatic source of the Santa Maria volcano has a composition similar to that of the local OIB-like mantle.
2. Santa Maria's main lava flow is composite (possibly 2 or more events formed the 17 km long basaltic flow)
3. U-series, geochemical analysis and petrographic observations show that Santa Maria's basaltic flow has not been affected by hydrothermal alteration and/or upper or lower continental crustal contamination.
4. We identify a differentiation trend in the Santa Maria products, which began from an already ^{226}Ra-enriched magma.
5. Fast magma ascent rates associated with channel flow are inferred.
6. The high ^{226}Ra excess over ^{230}Th is attributed to partial melting of different mantle domains with some input from the subducted-slab sediments.
7. A slight Andean arc signature has been determined for this Holocene volcano, which we interpret as the result of Chilean trench sediments being subducted, rather than arising directly from dehydration fluids of the subducting slab.

References

Berlo K, Turner S, Blundy J, Hawkesworth C (2004) The extent of U-series disequilibria produced during partial melting of the lower crust with implications for the formation of the Mount St. Helens dacites. Contributions to Mineralogy and Petrology 148:122-130

439 Boynton WV (1984) Cosmochemistry of the rare earth elements: meteoric studies. In
440 Rare Earth Element Geochemistry (ed. P Henderson): 63-114. Amsterdam, Elsevier

441 Chabaux F, Ben Othman D, Birck, J (1994) A new Ra-Ba chromatographic
442 separation and its application to Ra mass-spectrometric measurement in volcanic
443 rocks. Chemical Geology 114: 191-197.

444 Cheng H, Edwards R, Hoff J, Gallup C, Richards D, Asmerom Y (2000) The half-
445 lives of uranium-234 and thorium-230. Chemical Geology 169: 17-33

446 Claude-Ivanaj C, Bourdon B, Allègre CJ (1998) Ra–Th–Sr isotope systematics in
447 Grande Comore Island: a case study of plume–lithosphere interaction. Earth and
448 Planetary Science Letters 164:99-117

449 Condomines M, Sigmarsson O (1993) Why are so many arc magmas close to ^{238}U-
450 ^{230}Th radioactive equilibrium? Geochimica et Cosmochimica Acta 57:4491-4497

451 Espanon VR, Chivas AR, Kinsley LPJ, Dosseto A (2014a) Geochemical variations in
452 the Quaternary Andean back-arc volcanism, southern Mendoza, Argentina. Lithos
453 208–209:251-264

454 Espanon VR, Honda M, Chivas AR (2014b) Cosmogenic ^{3}He and ^{21}Ne surface
455 exposure dating of young basalts from Southern Mendoza, Argentina. Quaternary
456 Geochronology 19:76-86

457 Espanon VR, Chivas AR, Phillips D, Matchan EL, Dosseto A (2014c).
458 Geochronological, morphometric and geochemical constraints on the Pampas
459 Onduladas long basaltic flow (Payún Matrú Volcanic Field, Mendoza, Argentina).
460 Journal of Volcanology and Geothermal Research 289: 114-129

461 Gerlach, D, Frey, F, Moreno-Roa, H, Lopez-Escobar, L, (1988) Recent volcanism in
462 the Puyehue–Cordon Caulle region, southern Andes, Chile (40.5°S): petrogenesis of
463 evolved lavas. Journal of Petrology 29: 333–382

464 Germa A, Quidelleur X, Gillot PY, Tchilinguirian P (2010) Volcanic evolution of the
465 back-arc Pleistocene Payun Matru volcanic field (Argentina). Journal of South
466 American Earth Sciences 29:717-730

467 Gill, JB, Williams RW (1990) Th isotope and U-series studies of subduction-related
468 volcanic rocks. Geochimica et Cosmochimica Acta 54: 1427-1442

469 Gladney ES, Roelandts I (1988) 1987 Compilation of elemental concentration data
470 for USGS BIR-1, DNC-1, and W-2. Geostandards Newsletter 12:63-118

471 Gudnason J, Holm PM, Søager N, Llambías EJ (2012) Geochronology of the late
472 Pliocene to recent volcanic activity in the Payenia back-arc volcanic province,
473 Mendoza Argentina. Journal of South American Earth Sciences 37: 191-201

474 Hernando IR, Llambías EJ, González PD, Sato K (2012) Volcanic stratigraphy and
475 evidence of magma mixing in the Quaternary Payun Matru volcano, Andean backarc
476 in western Argentina. Andean Geology 39:158-179

477 Holden NE (1990) Total half-lives for selected nuclides. Pure and Applied Chemistry
478 62: 941-958

479 Jacques G, Hoernle K, Gill J, Hauff F, Wehrmann H, Garbe-Schönberg D, Van den
480 Bogaard P, Bindeman I, Lara LE (2013) Across-arc geochemical variations in the
481 Southern Volcanic Zone, Chile (34.5-38.0°S): Constraints on mantle wedge and slab
482 input compositions Geochimica et Cosmochimica Acta 123:218-243

Jaffey A, Flynn K, Glendenin L, Bentley W, Essling A (1971) Precision measurement of half-lives and specific activities of ^{235}U and ^{238}U. Physical Review C, 4: 1889-1906

Jochum KP, Weis U, Stoll B, Kuzmin D, Yang Q, Raczek I, Jacob DE, Stracke A, Birbaum K, Frick DA (2011) Determination of reference values for NIST SRM 610–617 glasses following ISO guidelines. Geostandards and Geoanalytical Research 35:397-429

Kay SM, Ardolino AA, Gorring ML, Ramos V.A. (2007) The Somuncura large igneous province in Patagonia: interaction of a transient mantle thermal anomaly with a subducting slab. Journal of Petrology 48:43-77

Koornneef JM, Stracke A, Aciego S, Reubi O, Bourdon B (2010) A new method for U–Th–Pa–Ra separation and accurate measurement of ^{234}U–^{230}Th–^{231}Pa–^{226}Ra disequilibria in volcanic rocks by MC-ICPMS. Chemical Geology 277:30-41

Le Bas M, Le Maitre R, Streckeisen A, Zanettin B (1986) A chemical classification of volcanic rocks based on the total alkali-silica diagram. Journal of Petrology 27:745-750

Le Roux LJ, Glendenin LE (1963) Half-life of ^{232}Th. Proc. Nat. Meet. Nucl. Energy, Pretoria, South Africa 83-94

Lundstrom CC, Hoernle K, Gill J (2003) U-series disequilibria in volcanic rocks from the Canary Islands: Plume versus lithospheric melting. Geochimica et Cosmochimica Acta 67:4153-4177

Luo X, Rehkämper M, Lee D-C, Halliday AN (1997) High precision 230Th/232Th and 234U/238U measurements using energy filtered ICP magnetic sector multiple

505 collector mass spectrometry. International Journal of Mass Spectrometry and Ion
506 Processes 171:105-117

507 McDonough WF, Sun S-S (1995) The composition of the Earth. Chemical Geology
508 120:223-253

509 Moffat I, 2013 Spatially resolved strontium isotope micro-analysis of lower and
510 middle Palaeolithic fauna from archaeological sites in Israel and southern France,
511 PhD thesis, The Australian National University, 1127pp.

512 Pasquarè G, Bistacchi A, Francalanci L, Bertotto G, Boari E, Massironi M, Rossotti A
513 (2008) Very long pahoehoe inflated basaltic lava flows in the Payenia Volcanic
514 Province (Mendoza and La Pampa, Argentina). Revista de la Asociación Geológica
515 Argentina 63:131-149

516 Reubi O, Sims KWW, Bourdon B (2014) ^{238}U-^{230}Th equilibrium in arc magmas and
517 implications for the time scales of mantle metasomatism. Earth and Planetary
518 Science Letters 391:146-158

519 Risso C, Nemeth K, Marti U (2006) Proposed geosites on Pliocene to Recent
520 pyroclastic cone fields in Mendoza, Argentina. Zeitschrift der Deutschen Gesellschaft
521 für Geowissenschaften 157/3:477-490

522 Rudnick RL, Gao S (2003) Composition of the continental crust. In the Crust (ed. RL,
523 Rudnick) Vol. 3 Treatise on Geochemistry (eds. HD, Holland and KK, Turekian),
524 Elsevier-Pergamon, Oxford, pp 1-64

525 Schmidt MW, Poli S (1998). Experimentally based water budgets for dehydrating
526 slabs and consequences for arc magma generation. Earth and Planetary Science
527 Letters 163: 361-379

528 Sigmarsson O, Chmeleff J, Morris J, Lopez-Escobar L (2002) Origin of ^{226}Ra-^{230}Th
529 disequilibria in arc lavas from southern Chile and implications for magma transfer
530 time. Earth and Planetary Science Letters 196:189-196

531 Sims KWW, Gill JB, Dosseto A, Hoffmann DL, Lundstrom CC, Williams RW, Ball L,
532 Tollstrup D, Turner S, Prytulak J, Glessner JJG, Standish JJ, Elliott T (2008) An
533 Inter-Laboratory assessment of the thorium isotopic composition of synthetic and
534 rock reference materials. Geostandards and Geoanalytical Research 32:65-91

535 Sims K, DePaolo D, Murrell M, Baldridge W, Goldstein S, Clague D, Jull M (1999)
536 Porosity of the melting zone and variations in the solid mantle upwelling rate beneath
537 Hawaii: inferences from ^{238}U-^{230}Th-^{226}Ra and ^{235}U-^{231}Pa disequilibria. Geochimica et
538 Cosmochimica Acta 63:4119-4138

539 Søager N, Holm PM, Llambías EJ (2013) Payenia volcanic province, southern
540 Mendoza, Argentina: OIB mantle upwelling in a backarc environment. Chemical
541 Geology 349-350:36-53

542 Søager N, Holm, PM (2013) Melt–peridotite reactions in upwelling eclogite bodies:
543 Constraints from EM1-type alkaline basalts in Payenia, Argentina. Chemical Geology
544 360: 204-219

545 Søager N, Holm PM, Thirlwall MF (2015) Sr, Nd, Pb and Hf isotopic constraints on
546 mantle sources and crustal contaminants in the Payenia volcanic province,
547 Argentina. Lithos 212: 368-378

548 Sun S-S, McDonough WF (1989) Chemical and isotopic systematics of oceanic
549 basalts: implications for mantle composition and processes. Geological Society,
550 London, Special Publications 42:313-345

551 Tassara A, Götze HJ, Schmidt S, Hackney R (2006) Three-dimensional density
552 model of the Nazca plate and the Andean continental margin. Journal of Geophysical
553 Research: 111 (B09404)

554 Turner S, Evans P, Hawkesworth C (2001) Ultrafast source-to-surface movement of
555 melt at island arcs from ^{226}Ra-^{230}Th systematics. Science 292: 1363-1366

556 Turner S, Bourdon B, Gill J (2003) Insights into magma genesis at convergent
557 margins from U-series isotopes. In: Bourdon B, Henderson GM, Lundstrom CC,
558 Turner S (eds), Uranium -Series Geochemistry, Reviews in Mineralogy and
559 Geochemistry. Mineralogical Society of America, Washington, pp 255-315

560 Varekamp J, Hesse A, Mandeville C (2010) Back-arc basalts from the Loncopue
561 graben (Province of Neuquen, Argentina). Journal of Volcanology and Geothermal
562 Research 197:313-328

563 Vigier N, Bourdon B, Joron J, Allègre C (1999) U-decay series and trace element
564 systematics in the 1978 eruption of Ardoukoba, Asal rift: timescale of magma
565 crystallization. Earth and Planetary Science Letters 174:81-98

566 Villemant B, Bourdon B, Komorowski J-C (1996) U-series disequilibrium in arc
567 magmas induced by water-magma interaction. Earth and Planetary Science Letters
568 140:259-267

569 Williams RW, Gill JB (1989) Effects of partial melting on the uranium decay series.
570 Geochimica et Cosmochimica Acta 53: 1607-1619

571 Wilson SA (1997) The collection, preparation and testing of USGS reference material
572 BCR-2, Columbia River, Basalt: US Geological Survey Open-File report 98

Figure captions

Fig. 1 Location of the Payenia Basaltic Province, Payún Matrú Volcanic Field and the Santa Maria volcano. a) Location of the Quaternary back-arc volcanic fields in Patagonia (modified after Kay et al. (2007). Payenia Basaltic Province (PBP), Loncopue (LP), Crater basalt (CB), Sierra de San Bernardo (SSB), Meseta del Lago Buenos Aires (MLBS) and Pali Aike (PA). The Somuncura Plateau is the only Neogene Patagonian basaltic field shown. SVZ = Southern Volcanic Zone and AVZ = Austral Volcanic Zone. b) Detail of the Payenia Basaltic Province showing the four main volcanic fields, Llancanelo (LLVF), Nevado (NVF), Payún Matrú (PMVF) and Río Colorado (RCVF) (based on Gudnason et al. 2012). c) Santa Maria volcano and emitted basaltic flow with sample locations. Green dots indicate samples used for general geochemical analysis (major and trace elements) and for U-series disequilibria; blue dot samples used for general geochemistry only. Note that samples VRE51 and VRE52 share the same location, as the two samples were taken within a couple of metres but from different material. Base images from Gtopo 30 (Global 30 Arc-Second Elevation Data Set), GEBCO 08 grid and Landsat 7.

Fig. 2 Field images of the Santa Maria volcanic cone, flow and pyroclastic material. a) View of Santa Maria main cone and flow. Note the high angle of the main cone, and its crater breached to the NW. b) Ribbon-type pyroclastic bomb. c) Bread-crust pyroclastic bomb. d) View from the inner part of the main crater to the NW showing part of the collapsed ramparts. In the background, one of the eruption points is present as a fissure. e) Upper part of the main Santa Maria cone. Note the light colours possibly indicating an extinct fumarole or solfatara. f) Inner part of Santa Maria's main flow showing the two generations of basaltic flow (note that flow 1 underlies flow 2). g) Inner part of the flow showing the typical a'a style of the flow. h)

598 Inner part of the Santa Maria flow close to the SM3 sampling site (Figure 1c),
599 showing tube-like structures. Person for scale.

600 Fig. 3 Normalised trace-element diagrams. a) Rare Earth Element (REE)
601 concentrations normalised to chondrite (Boynton, 1984). b) Sample concentrations
602 normalised to primitive mantle values from McDonough and Sun (1995). The Río
603 Colorado field (shaded field) represents the local intraplate end-member with an
604 OIB-like composition (Søager et al. 2013) from the southern PBP. The arc end-
605 member (dashed line) is the average from the Andean volcanic arc with <53 SiO_2 wt
606 % between 35°S and 38°S (See Espanon et al., 2014a for references).

607 Fig. 4 U-Th-Ra disequilibria. a) ($^{230}Th/^{232}Th$) vs ($^{238}U/^{232}Th$); b) ($^{234}U/^{238}U$); c)
608 ($^{226}Ra/^{230}Th$) vs Rb/Th; d) ($^{226}Ra/^{230}Th$) vs Th (ppm) ; e) (^{226}Ra)/Ba (in dpm/ųg) vs
609 (^{230}Th)/ Ba (in dpm/ųg) and f) ($^{230}Th/^{238}U$) vs La/Yb. The parentheses signify activity
610 ratios, unless otherwise specified. The equiline represents secular equilibrium
611 between the parent and the daughter isotope. The arrows indicate the effects of
612 different processes on the lavas. Differentiation represents the change in
613 composition while fractional crystallisation is a process to create differentiation. Note
614 that the ^{226}Ra excess has not been corrected for the decay since eruption, as precise
615 eruption ages are unknown. Dark green squares reflect the hypothesized flow 2.

616 Fig. 5 Trace-element ratios. a) Zr (ppm) vs Y (ppm); b) $K_2O + Na_2O$ vs SiO_2; c) Cr/Th
617 vs MgO; d) Ce/Pb vs Nb/U; e) Th/Nb vs La/Nb; f) Ba/Th vs U/Pb. The Río Colorado
618 field is from Søager et al. (2013), the Payún Matrú volcanic field is from Espanon et
619 al. (2014), the Chilean trench sediments are from Jacques et al. (2013). The lower
620 (LCC) and the upper (UCC) continental crust squares are from Rudnick and Gao
621 (2003). The volcanic arc field corresponds to an average from the Andean volcanic

622 arc with <53 SiO2 wt % between 35°S and 38°S (See Espanon et al., 2014a for
623 references). The lines in d) and e) represent a correlation between Chilean trench
624 sediments, Rio Colorado and Santa Maria data points. Note that including the UCC
625 point in the correlation has only an effect on the 3rd r^2 decimal place.

626

Table captions

Table 1. Major- and trace-element concentrations and Sr-isotopic composition for selected samples from the Santa Maria volcano.

Table 2. U-Th-Ra disequilibria for basaltic samples from the Santa Maria volcano.

Figure 1

Click here to download Figure Figure 1.tif

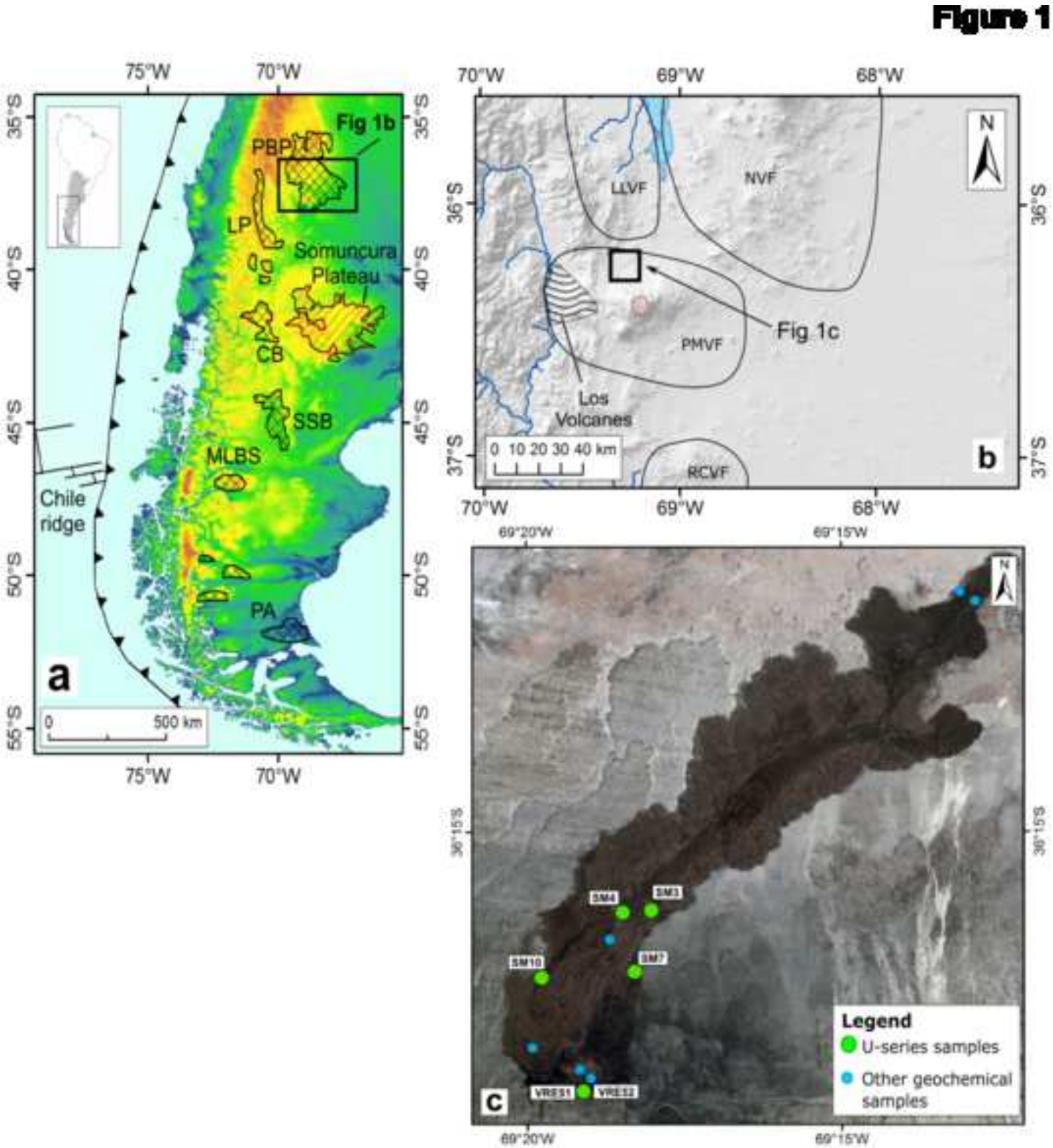

Figure 2

Click here to download Figure Figure 2.tif

Figure 3

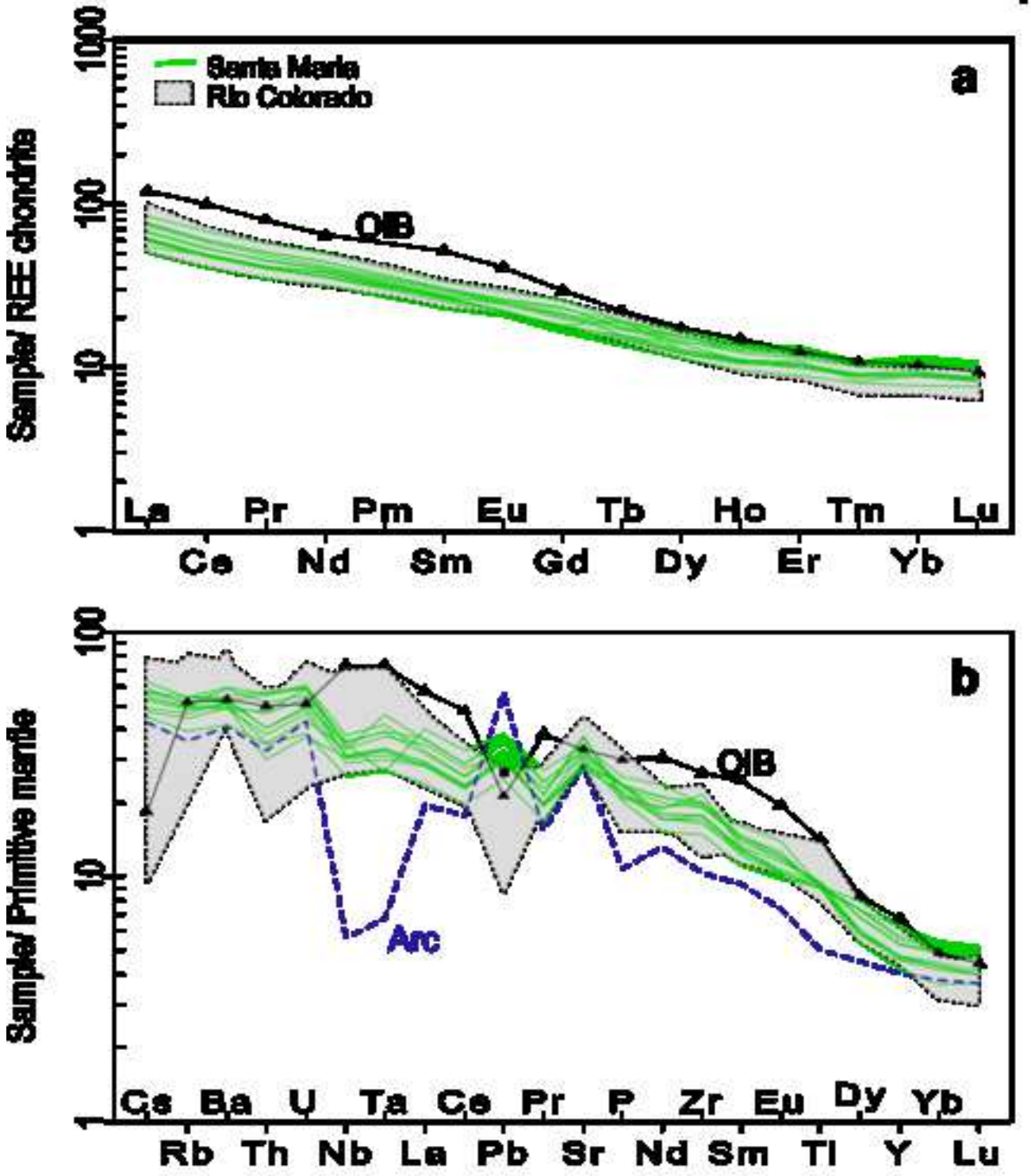

Figure 4

Click here to download Figure Figure 4.tif

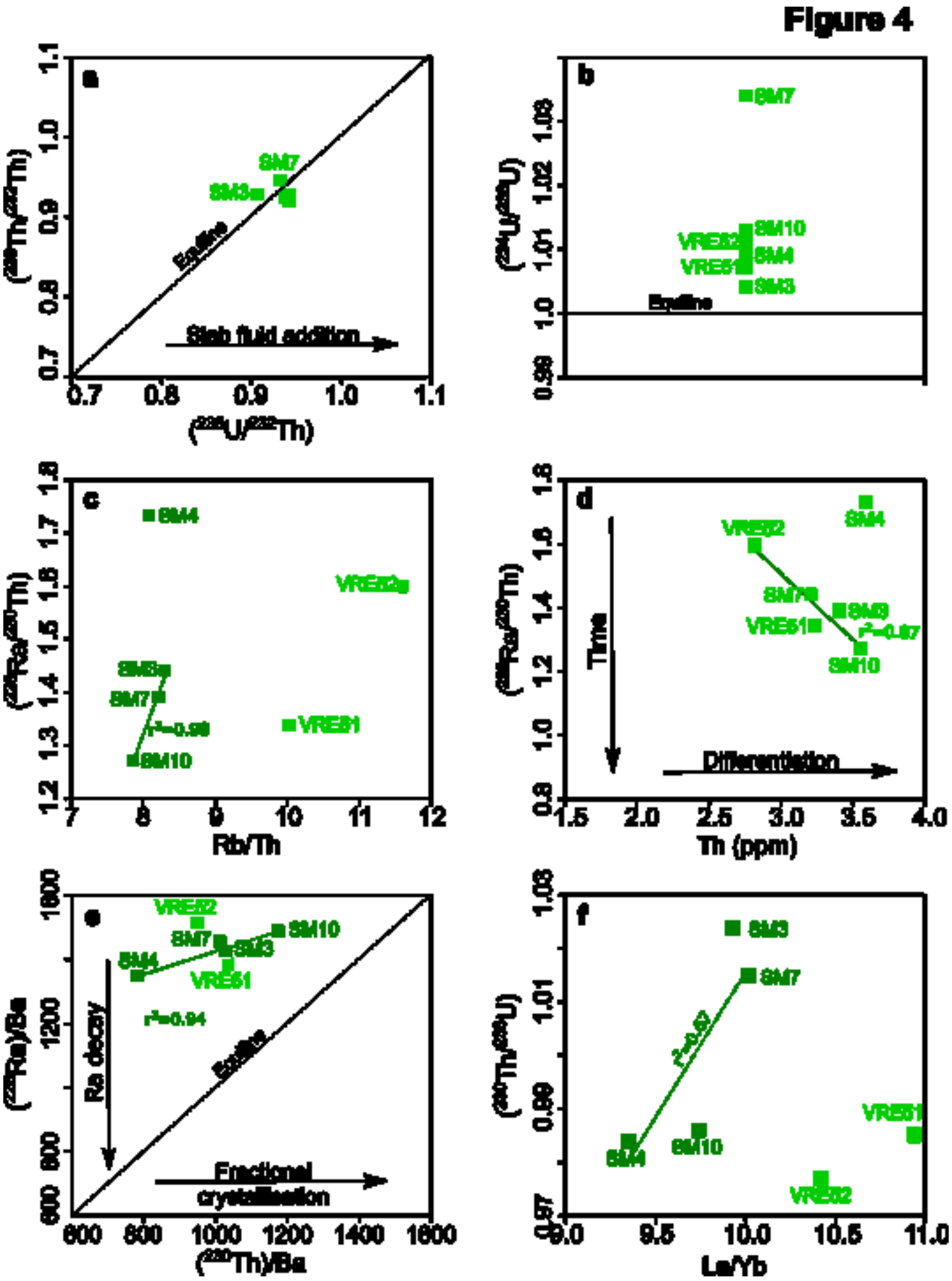

Figure 5

Click here to download Figure Figure 5.tif

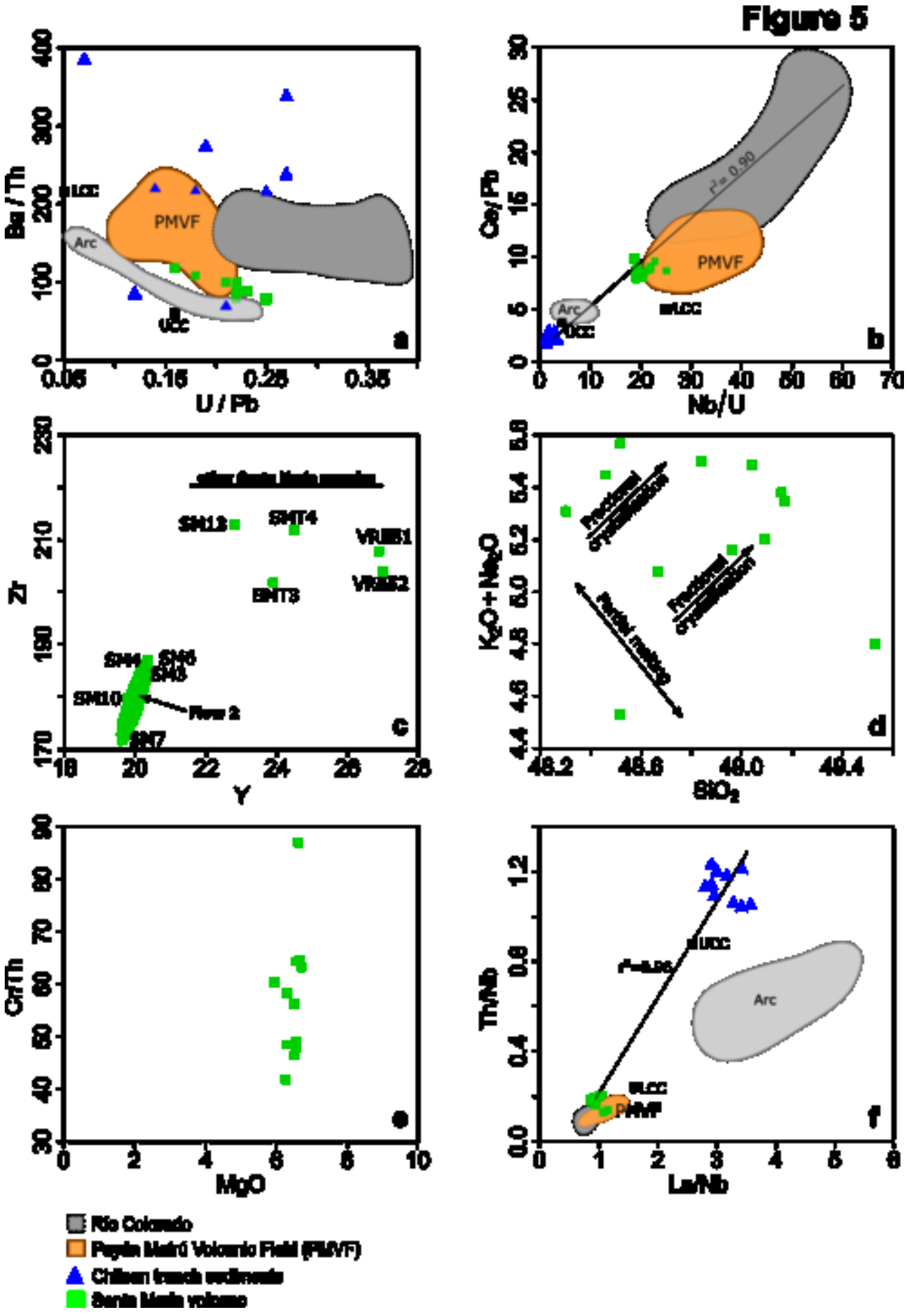

Table 1. Major- and trace-element concentrations and Sr-isotopic composition for selected samples from the Santa Maria volcano.

Sample	**SM3**	**SM4**	**SM6**	**SM7**	**SM9**	**SM10**
Material	Basalt	Basalt	Basalt	Basalt	Scoria	Basalt
Latitude	-36.2669	-36.2674	-36.2732	-36.2802	-36.2966	-36.2814
Longitude	-69.3005	-69.3080	-69.3114	-69.3049	-69.3320	-69.3296
Elevation (MASL)	1634	1635	1664	1660	1793	1723
SiO_2	48.71	49.03	48.91	48.17	48.39	49.05
TiO_2	1.91	1.81	1.80	1.87	1.83	1.80
Al_2O_3	17.50	16.95	16.98	17.05	17.45	16.84
Fe_2O_3	10.16	10.45	10.52	10.78	10.43	10.52
MnO	0.14	0.15	0.15	0.15	0.14	0.15
MgO	5.92	6.53	6.48	6.65	6.63	6.67
CaO	9.40	9.01	8.91	9.29	9.91	8.92
Na_2O	4.01	3.89	3.95	3.87	3.33	3.87
K_2O	1.48	1.48	1.52	1.42	1.19	1.47
P_2O_5	0.49	0.44	0.49	0.49	0.42	0.46
LOI	0.18	0.00	0.00	0.00	0.66	0.00
V	236	228	225	233	238	225
Cr	206	231	209	208	241	239
Ni	96.0	94.7	89.3	94.1	103	104
Cu	49.50	45.2	45.5	48.0	46.4	48.9
Zn	51.7	54.2	54.3	54.9	52.7	56.6
Ga	20.0	20.4	19.7	20.0	19.5	19.6
Rb	28.0	28.9	30.0	26.6	23.6	29.6
Sr	640	563	565	584	605	548
Y	20.3	20.3	20.4	19.6	18.0	19.8
Zr	185	187	187	172	155	180
Nb	20.7	20.2	20.4	19.2	16.9	19.9
Cs	1.03	1.10	1.14	0.99	0.94	1.14
Ba	343	329	330	321	277	319
Sc	25.7	25.5	25.0	25.5	26.9	24.9
La	18.9	18.4	19.1	18.4	15.6	18.6
Ce	39.5	38.1	39.7	38.5	33.0	38.5
Pr	5.07	4.91	5.05	5.00	4.27	4.90
Nd	22.5	21.4	22.6	21.5	19.2	21.4
Sm	5.27	5.30	5.10	5.17	4.51	4.94
Eu	1.64	1.59	1.61	1.58	1.51	1.54
Gd	4.57	4.64	4.66	4.45	4.22	4.35
Tb	0.74	0.91	0.73	0.70	0.64	0.70
Dy	4.11	4.11	3.98	3.96	3.63	3.87
Ho	0.79	0.80	0.78	0.76	0.68	0.75
Er	2.12	2.13	2.19	2.07	1.86	2.15
Tm	0.29	0.30	0.29	0.28	0.26	0.29
Yb	1.90	1.97	1.88	1.84	1.61	1.91
Lu	0.27	0.28	0.27	0.27	0.25	0.27
Hf	4.28	4.36	4.37	3.98	3.64	4.20
Ta	1.23	1.21	1.22	1.11	1.01	1.16
Pb	4.37	4.53	4.57	4.41	3.76	4.81
Th	3.24	2.42	3.70	3.04	2.77	3.77
U	0.97	0.75	1.07	0.93	0.77	1.17
$^{87}Sr/^{86}Sr$		0.703861				0.703867

Table 1. cont.

Sample	SM12	SM13	SMT3	SMT4	VRE51	VRE52
Material	Scoria	Basalt	Basalt	Basalt	Bomb	Basalt
Latitude	-36.3032	-36.2948	-36.2002	-36.1981	-36.3060	-36.3060
Longitude	-69.3165	-69.3186	-69.2145	-69.2186	-69.3185	-69.3185
Elevation (MASL)	1848	1774	1534	1517	1811	1811
SiO_2	49.41	48.54	48.36	48.74	48.03	48.14
TiO_2	1.91	1.91	1.81	1.85	1.81	1.77
Al_2O_3	17.44	17.13	16.36	17.03	16.93	16.84
Fe_2O_3	10.77	10.77	10.91	10.89	10.42	10.42
MnO	0.15	0.15	0.16	0.16	0.15	0.16
MgO	6.23	6.52	6.43	6.53	6.17	6.17
CaO	8.48	9.22	8.89	9.12	8.97	8.97
Na_2O	3.36	3.61	3.82	4.04	3.58	3.65
K_2O	1.43	1.45	1.51	1.56	1.49	1.46
P_2O_5	0.44	0.43	0.47	0.49	0.52	0.47
LOI	0.27	0.00	0.00	0.00	0.00	0.00
V	233	249	225	231	212	214
Cr	187	197	218	213	158	165
Ni	80.4	95.1	96.0	92.6	67.5	67.5
Cu	34.7	40.5	44.1	49.4	45.7	48.1
Zn	56.3	58.8	58.7	58.2	90.3	91.5
Ga	21.0	21.0	20.0	20.5	21.4	20.7
Rb	32.4	30.7	31.2	32.3	32.5	32.7
Sr	734	749	617	661	687	647
Y	22.6	22.8	23.9	24.5	26.9	27.0
Zr	228	213	202	212	208	204
Nb	24.7	23.5	22.0	23.1	22.8	21.8
Cs	1.31	1.23	1.19	1.20	N/A	N/A
Ba	390	389	345	362	351	335
Sc	27.3	27.6	25.6	25.5	21.9	21.9
La	21.1	20.6	22.7	23.7	26.2	23.5
Ce	43.2	42.8	46.6	48.4	54.7	48.5
Pr	5.48	5.50	5.85	6.14	6.92	6.21
Nd	23.6	24.0	25.0	26.4	29.8	26.5
Sm	5.39	5.69	5.85	5.96	6.52	5.96
Eu	1.77	1.82	1.83	1.88	2.14	1.93
Gd	5.11	5.24	5.44	5.83	6.63	6.03
Tb	0.81	0.85	0.88	0.91	0.90	0.82
Dy	4.57	4.64	4.91	4.97	5.35	4.94
Ho	0.92	0.88	0.96	0.96	0.97	0.90
Er	2.46	2.40	2.58	2.62	2.80	2.61
Tm	0.34	0.33	0.35	0.35	0.35	0.33
Yb	2.16	2.21	2.26	2.32	2.39	2.26
Lu	0.33	0.31	0.34	0.33	0.35	0.33
Hf	5.52	5.18	4.95	5.07	N/A	N/A
Ta	1.55	1.44	1.38	1.45	1	1.7
Pb	5.37	4.92	4.74	5.45	5.7	5.6
Th	4.45	4.13	4.43	4.58	3.24	2.82
U	1.21	1.10	1.17	1.19	1.00	0.87
$^{87}Sr/^{86}Sr$						

The major element concentrations are in wt % and the trace element concentrations are in ppm. Errors are <3 % and <5 % (2σ), respectively.

Table 2

Table 2. U-Th-Ra disequilibria for basaltic samples from the Santa Maria volcano

Sample	[Ra] (fg/g)	$(^{230}Th/^{232}Th)^a$	Error	$(^{238}U/^{232}Th)^b$	Error	$(^{230}Th/^{238}U)$	Error	$(^{234}U/^{238}U)^c$	Error	$(^{226}Ra/^{230}Th)^d$	Error
SM3	466	0.929	0.002	0.907	0.017	1.024	0.003	1.004	0.019	1.391	0.005
SM4	433	0.928	0.002	0.943	0.006	0.984	0.002	1.009	0.006	1.732	0.043
SM7	460	0.946	0.002	0.932	0.006	1.015	0.003	1.034	0.006	1.440	0.006
SM10	493	0.925	0.004	0.938	0.008	0.986	0.004	1.013	0.008	1.270	0.004
VRE51	447	0.927	0.003	0.941	0.008	0.985	0.003	1.007	0.008	1.339	0.007
VRE52	461	0.920	0.001	0.942	0.005	0.977	0.001	1.011	0.005	1.598	0.006

[a] Based on λ_{230}= 9.158 x 10^{-6} yr^{-1} (Cheng et al. 2000) and λ_{232}= 4.948 x 10^{-11} yr^{-1} (Le Roux and Glendenin 1963)

[b] Based on λ_{238}= 1.551 x 10^{-10} yr^{-1} (Jaffey et al. 1971)

[c] Based on λ_{234}= 2.826 x 10^{-6} yr^{-1} (Cheng et al. 2000)

[d] Based on λ_{226}= 4.332 x 10^{-4} yr^{-1} (Holden 1990)